The secreted neuronal signal Spock1 regulates the blood-brain barrier

Natasha M. O'Brown[1*], Nikit B. Patel[1], Ursula Hartmann[2], Allon M. Klein[1], Chenghua Gu[3], Sean G. Megason[1*]

[1] Department of Systems Biology, Harvard Medical School, 200 Longwood Ave, Boston, MA 02115, U.S.A.
[2] University of Cologne, Joseph-Stelzmann-Str. 52 50931 Cologne, Germany
[3] Howard Hughes Medical Institute, Department of Neurobiology, Harvard Medical School, 220 Longwood Ave, Boston, MA 02115, USA

* denotes corresponding author

Correspondence:

Natasha M. O'Brown (Natasha_obrown@hms.harvard.edu)
Department of Systems Biology, Harvard Medical School
Boston, MA 02115, U.S.A.

Sean G. Megason (megason@hms.harvard.edu)
Department of Systems Biology, Harvard Medical School
Boston, MA 02115, U.S.A.
(Phone) 617-432-7441

Abstract

The blood-brain barrier (BBB) is comprised of a single layer of endothelial cells with uniquely restrictive properties required for maintaining a tightly controlled homeostatic environment in the brain. Classic quail-chick grafting experiments showed that BBB properties are not intrinsic to brain endothelial cells, but instead are induced by signals from the embryonic brain microenvironment. Here we have identified a neuronally produced signal, Spock1, that specifically regulates BBB functional development in both zebrafish and mice without affecting angiogenesis. Using a combination of mosaic genetic analysis, tracer leakage assays and live imaging we show that Spock1 from neurons can regulate brain vasculature permeability non-cell autonomously. Electron microscopy analyses of *spock1* mutants revealed that the leakage arises predominantly through increased endothelial transcytosis of both clathrin-independent small and large vesicles due to altered pericyte-endothelial interactions. Single-cell RNA sequencing analyses revealed a reduction in vascular expression of the cell adhesion molecule *mcamb* in the *spock1* mutants, and this down-regulation of *mcamb* occurred specifically in regions with increased BBB leakage. These analyses indicate that the neuronal signal Spock1 regulates BBB properties by altering vascular gene expression and cellular interactions.

The blood-brain barrier (BBB) maintains a tightly controlled homeostatic environment in the brain that is required for proper neural function. BBB breakdown has been implicated in multiple neurodegenerative diseases including Alzheimer's, Parkinson's and Huntington's Diseases[1]. Conversely, the BBB also serves as a barrier for drug delivery to the brain, prompting interest in understanding how to therapeutically regulate its permeability. The BBB is a specialized property of the brain vasculature, which is composed of a thin, continuous layer of non-fenestrated endothelial cells with uniquely restrictive properties. Brain endothelial cells create the barrier via two primary cellular mechanisms: 1) specialized tight junction complexes that block the transit of small water-soluble molecules between cells and 2) reduced levels of vesicular trafficking or transcytosis to restrict transit through endothelial cells[2]. Classic quail-chick chimera experiments showed that these restrictive properties are not intrinsic to BBB endothelial cells, but rather are acquired during development through their interactions with signals in the brain microenvironment[3]. Furthermore, these microenvironmental signals are also required to actively maintain these restrictive properties[4–8]. Wnt signaling arising from both neuronal and astrocytic sources is the only microenvironmental signal shown to induce and maintain BBB function[8–14]. However, it is likely only one of many signals that regulate BBB properties and plays roles in both angiogenesis and barriergenesis[11,12].

We previously characterized the molecular and subcellular mechanisms of functional BBB development in the optically accessible vertebrate zebrafish[15]. During these studies, we serendipitously discovered a recessive mutant with forebrain and midbrain barrier leakage of both an injected 1 kDa Alexa Fluor (AF) 405 NHS Ester and a transgenic 80 kDa serum protein DBP-EGFP[16] at 5 days post fertilization (dpf), when the wild type BBB is functionally sealed (Fig. 1a-c)[15]. Mutants exhibit increased vascular permeability as early as 3 dpf with no improvement in BBB function throughout larval development (Extended Data Fig. 1). This increased BBB permeability in homozygous mutants occurs the absence of hemorrhage or vascular patterning defects (Extended Data Fig. 2), alterations in neural activity (Extended Data Fig. 3), or any reduction in viability or fertility. Time lapse imaging of injected 10 kDa Dextran revealed a steady accumulation of Dextran in the brain parenchyma of leaky mutants over the course of an hour (Extended Data Fig. 4), closely resembling the dynamics of Dextran leakage observed in *mfsd2aa* mutants with increased endothelial transcytosis[15].

To identify the mutation responsible for this leakage phenotype, we performed linkage mapping on 5 dpf mutant and wild type siblings using bulk segregant RNAseq[17] and identified a single peak at chr14:2205271-3513919 (GRCz11; Fig. 1d, Extended Data Fig. 5). Of the 14 genes within the linkage region (Extended Data Fig. 5), 8 were expressed at 5 dpf. Two of these genes were differentially expressed, *csf1ra* and *gstp2* (Extended Data Table 1), and one had several mutations that fully segregated with the leakage phenotype, *spock1.* To test whether loss of any of these genes conferred the increased BBB permeability, we assessed tracer leakage in mosaic crispants (zebrafish larvae injected at the 1-cell stage with Cas9 protein and gene-specific sgRNAs) at 5 dpf and observed no BBB defects in 42 *gstp2* or 35 *csf1ra* crispants (data not shown). However, when we assessed BBB function in *spock1* crispants, we observed a strong leaky phenotype in 26% of larvae (26/100 injected fish; Fig. 1h #3) and moderate leakage in 53% (53/100 injected fish; Fig. 1h #1). Strikingly, a few of the crispants displayed BBB leakage restricted to one midbrain hemisphere (4/100 injected fish; Fig. 1h #2). *Spock1* encodes a secreted protein of unclear function named for its conserved protein domains: SPARC (Osteonectin), Cwcv And Kazal Like Domains Proteoglycan 1 protein (also known as Testican-1). Spock1 has three predicted domains: 1) a Kazal-type serine protease inhibitor, 2) an extracellular SPARC calcium-binding region, and 3) a thyroglobulin type-1 repeat region, in addition to being decorated by both chondroitin sulfate (CS) and heparan sulfate (HS) glycosaminoglycan (GAG) chains (Fig. 1e)[18,19]. Deeper sequencing of *spock1* revealed a few point mutations in the SPARC calcium-binding domain in the leaky fish (Fig. 1g), hereafter referred to as s*pock1*$^{hm41/hm41}$ mutants.

To determine whether or not Spock1 plays a conserved role in determining vertebrate BBB properties, we assessed BBB function in embryonic day 15.5 (E15.5) mice (Fig. 1i), when the cortex BBB is fully functional[20]. While wild type siblings confined both 550 Da Sulfo-NHS-Biotin (Fig. 1j) and 10 kDa Dextran (Fig. 1l) within the brain vasculature, *Spock1*$^{-/-}$ mice leaked both tracers into the cortex parenchyma (Fig. 1j-m, Extended Data Fig. 6). This increased BBB permeability was associated with increased expression of the plasmalemma vesicle-associated protein (PLVAP) (Extended Data Fig. 6), a structural protein that comprises the diaphragm in endothelial fenestrae and transcytotic vesicles[21]. When we repeated these leakage assays in adult mice, we observed full recovery in BBB function in *Spock1*$^{-/-}$ mice (Extended Data Fig. 7). This contrasts with adult zebrafish *spock1*$^{hm41/hm41}$ mutants, which continue to leak the serum protein into the brain (Extended Data Fig. 7), indicating species-specific differences in BBB maintenance.

Given the necessity of Spock1 in determining BBB function, we next wanted to assess where *spock1* was expressed during BBB development. Using HCR fluorescent *in situ* hybridization, we determined that *spock1* mRNA is expressed throughout the developing central nervous system, including the brain, retina and spinal cord (Extended Data Fig. 8), and that this expression is unaltered in *spock1*$^{hm41/hm41}$ mutants (Extended Data Fig. 9). Closer examination of the fluorescent signal revealed co-localization with the neuronal marker *elavl3* and not the vascular marker *kdrl* (Fig. 1n), similar to its predominantly neural expression in the developing mouse CNS[22]. Prior single-cell RNA sequencing (scRNA-seq) data[23] and our own also showed expression of *spock1* primarily in neurons and never in vascular endothelial cells (Extended Data Fig. 10). Taken together, these data indicate that we have identified a neuronal signal, Spock1, that plays a conserved role in establishing endothelial BBB properties during development without altering vascular patterning.

To test the ability of Spock1 to rescue the mutant leakage phenotype, we injected recombinant human SPOCK1 (rSPOCK1) protein directly into the brain of mutant larvae at 5 dpf and assessed brain permeability at 6 dpf. While control animals injected with 1 kDa AF 405 NHS Ester

maintained high levels of brain permeability (Fig. 2a), larvae that received at least 2.3 ng of rSPOCK1 per mg fish body weight showed a 50% reduction in brain permeability following a single dose (Fig. 2b,c). These results indicate that the leakage observed in the leaky mutants is due to loss of Spock1 activity and that SPOCK1 is able to act non-cell autonomously to rescue the mutant BBB leakage, as these injections were targeted broadly to the neural tissue rather than the endothelial cells.

To determine the range of the Spock1 signal, we performed cell transplantation experiments in zebrafish embryos and assessed tracer leakage in relationship to the closest transplanted cells at 5 dpf (Fig. 2d). When we transplanted wild type cells into wild type host embryos, we observed a negligible level of tracer accumulation in the brain parenchyma regardless of the proximity of the nearest donor cell (Fig. 2f). In contrast, when we transplanted *spock1*$^{hm41/hm41}$ mutant cells into mutant host embryos, we observed high levels of tracer accumulation in the parenchyma regardless of the proximity of the nearest donor cell (Fig. 2f). Strikingly, when we transplanted wild type cells into *spock1* mutant hosts, we observed a complete rescue of the mutant leakage if the wild type donor cell was within 10 µm of a blood vessel and no rescue if the donor cell was more than 20 µm away (Fig. 2e,f), indicating that the functional range of Spock1 falls between 10 and 20 µm. Importantly, wild type cells could rescue leakage in mutant hosts when they differentiate as neurons but not endothelial cells (Fig. 2e).

To assess the subcellular mechanism of increased BBB permeability in *spock1*$^{hm41/hm41}$ mutants, we injected electron-dense NHS-gold nanoparticles (5 nm) into circulation, followed by transmission electron microscopy (TEM) imaging in 7 dpf *spock1* mutant and wildtype siblings (Fig. 3). These TEM leakage assays revealed no alterations in the cellular composition of the neurovascular unit in *spock1* mutants, with endothelial cells and pericytes sharing a basement membrane that is surrounded by neurons and glia (Fig. 3a-b). A modest impairment in tight junction function was observed in *spock1* mutants (52/59 functional tight junctions) compared to wild type siblings (57/57; Fig. 3b). However, *spock1* mutants had a significant increase in both small (<100 nm diameter) non-clathrin coated vesicles (Fig. 3b, d) and large (>200 nm diameter) vesicles (Fig. 3c, e) suggesting that the leakage results primarily from an increase in vesicular trafficking across endothelial cells. In addition to the increase in total large vesicular abundance in *spock1* mutants, we also observed several of these large vesicles fused to the abluminal membrane in multiple larvae with a few examples of the gold nanoparticles visibly spilling into the endothelial basement membrane (Fig. 3c). Although pericyte coverage of the endothelium was unaltered (Extended Data Fig. 2), *spock1* mutants displayed overall thinner pericyte-endothelial basement membranes with several pericytes having long stretches of direct contact on endothelial cells (Fig. 3f-g). These data suggest that loss of Spock1 function alters the critical pericyte extracellular interactions with endothelial cells, resulting in loss of BBB properties as observed in pericyte-deficient mice and zebrafish[24–27].

To determine how Spock1, a neuronally produced and secreted proteoglycan, signals to and regulates brain endothelial cell BBB properties, we turned to scRNA-seq of dissected 5 dpf *spock1*$^{hm41/hm41}$ mutant and wild type brains, allowing us to reveal all cell type specific molecular changes occurring in the mutant brains. With Leiden clustering of the scRNA-seq data we defined cell clusters containing neurons, glial, and vascular cell types (Extended Data Fig. 10). We performed differential gene expression (DGE) analysis for each cluster and did not observe any changes in the neuronal or glial populations, but did observe significant changes in the vascular cluster (Extended Data Table 2). When we subclustered the vascular population, we were able to resolve endothelial cells, pericytes and vascular smooth muscle cells (vSMCs; Fig. 4a). Due to the low vascular cell numbers present in the scRNA-seq data, we prioritized candidate genes for subsequent validation by their fold-change in gene expression and not statistical significance.

These analyses suggested molecular changes in the mutant endothelial cells indicative of a leaky phenotype, with increased expression of *plvapb* and decreased expression of the tight junction protein *cldn5b* (Fig. 4b, Extended Data Table 3), as expected from the TEM analyses. Interestingly, *spock1* mutants had decreased expression of the melanoma cell adhesion molecule *mcamb* (also known as CD146) in both endothelial cells and pericytes (Fig. 4b-c). This decreased expression in the vasculature was validated by HCR FISH, with minimal expression in mutant midbrain pericytes but normal levels in the hindbrain pericytes, which maintain BBB function in *spock1*$^{hm41/hm41}$ mutants (Fig. 4d-g). CD146 has previously been shown to be required for BBB integrity, as *CD146*$^{-/-}$ mice exhibit BBB breakdown due to decreased pericyte coverage and downstream loss of endothelial expression of Cldn5[28].

In summary, Spock1 is a secreted, neuronally expressed signal that regulates BBB permeability in zebrafish and mouse without altering vascular patterning. Mechanistically, this work suggests a model whereby Spock1 regulates vascular expression of *mcamb*, whose main role is to ensure vascular cell connectivity, which in turn regulates vesicular transport across endothelial cells. Thus, loss of Spock1 function contributes to increased BBB permeability in part due to disruption of critical pericyte-endothelial cell contacts required for the establishment and maintenance of BBB properties. Together this work reveals how signals from the brain microenvironment can regulate the vasculature to give rise to the special properties of the BBB and provides new targets for its therapeutic modulation.

Acknowledgments

We thank members of the Megason laboratory for data discussion and comments on the manuscript; Dr. Zach O'Brown for discussions and comments on the manuscript; Ignas Mazelis for single cell demultiplexing software; the HMS Single Cell Core for single cell library preparation; Dr. Bela Anand-Apte (Cleveland Clinic) for providing the transgenic *l-fabp:DBP-EGFP* fish line (Xie et al., 2010) and Dr. Leonard Zon for providing the transgenic Tg(*kdrl:HRAS-mCherry*) line; and the HMS Electron Microscopy Core Facility, with special thanks to Louise Trakimas for all of her assistance in preparing the TEM samples. This work was supported by the Damon Runyon Cancer Foundation (N.M.O.), NIH R01HD096755 (S.G.M), an Allen Distinguished Investigator Award (C.G.), NIH R35NS116820 (C.G), and partially supported by Faculty Scholar grant from the Howard Hughes Medical Institute (C.G.). C.G. is an investigator of the Howard Hughes Medical Institute.

Author Contributions

N.M.O., S.G.M. and C.G. conceived the project and designed experiments. N.M.O. performed all experiments and analyzed most data with the exception of the scRNA-seq which was performed in collaboration with and analyzed by N.B.P. and A.M.K. U.H. provided the *Spock1*$^{-/-}$ mice. N.M.O., S.G.M. and C.G wrote the manuscript.

Fig. 1. The neuronal signal Spock1 plays a conserved role in establishing BBB function.

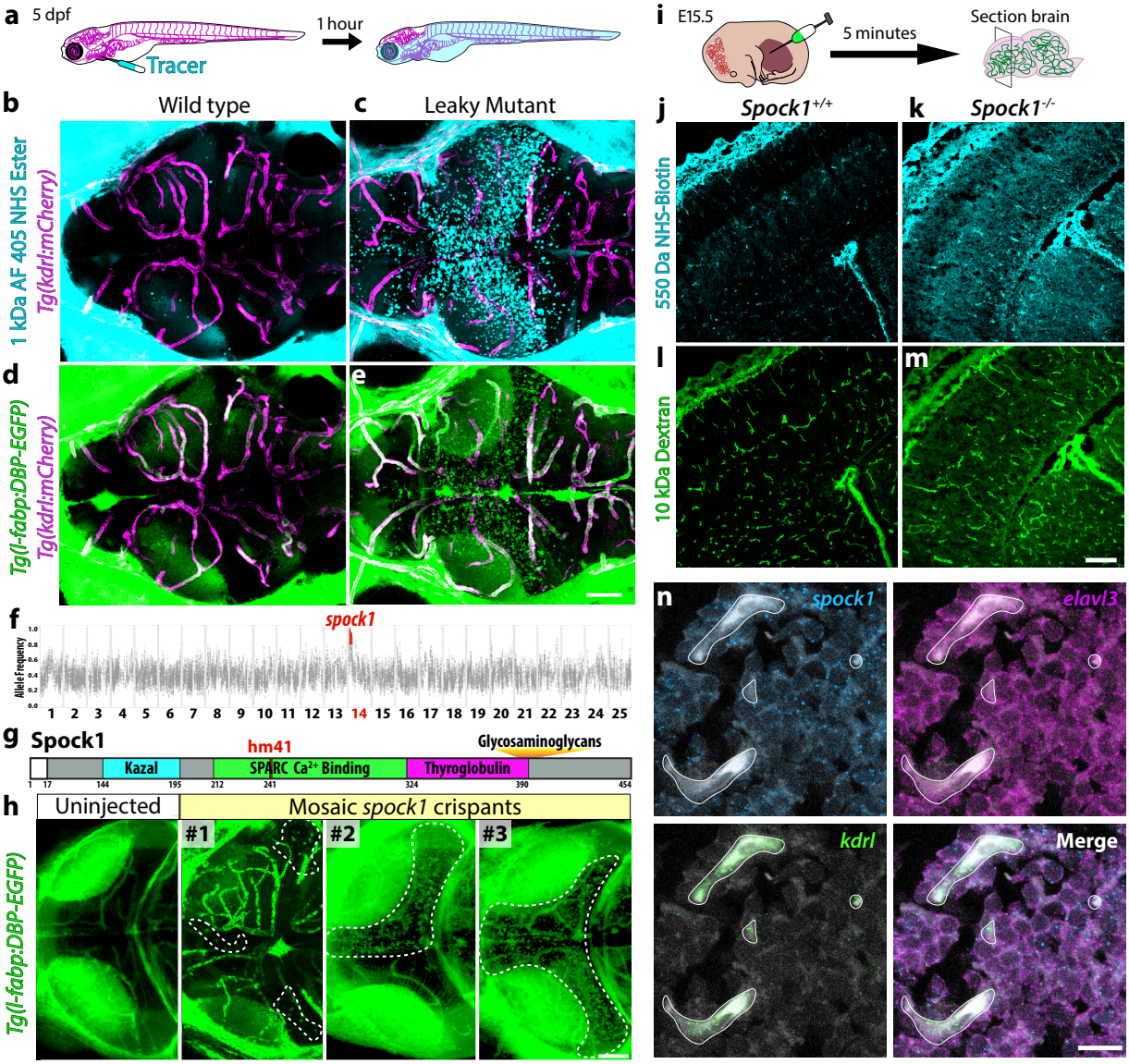

a-e, Fluorescent tracer leakage assays in 5 dpf zebrafish reveal BBB leakage in the forebrain and midbrain of both injected 1 kDa Alexa Fluor (AF) 405 NHS Ester (**c**) and 80 kDa DBP-EGFP (**e**) of mutant larvae compared to wild type controls (**b, d**). **f-g**, Linkage mapping of leaky phenotype reveals tight linkage to *spock1* on chromosome 14. *Spock1*^{hm41} mutants have several point mutations in the SPARC domain of Spock1 (**g**). **h**, CRISPR mutagenesis confirms that loss of Spock1 function results in increased BBB leakage in the mosaic *spock1* crispants. **i-m**, Tracer leakage assays in E15.5 *Spock1*$^{-/-}$ mice (**i**) reveal a conserved role for Spock1 in regulating BBB function, as *Spock1*$^{-/-}$ mice also leak injected 550 Da NHS-Biotin (**k**) and 10 kDa Dextran (**m**) tracers into the brain parenchyma. **n**, HCR fluorescent *in situ* hybridization reveals *spock1* (blue) localization within *elavl3* (magenta) positive neurons but not *kdrl* expressing blood vessels (green). Tissue and red blood cell autofluorescence is shown in grey. Scale bars represent 100 µm (**e, h, m**) and 10 µm (**n**).

Fig. 2. Spock1 regulates endothelial cells non-autonomously.

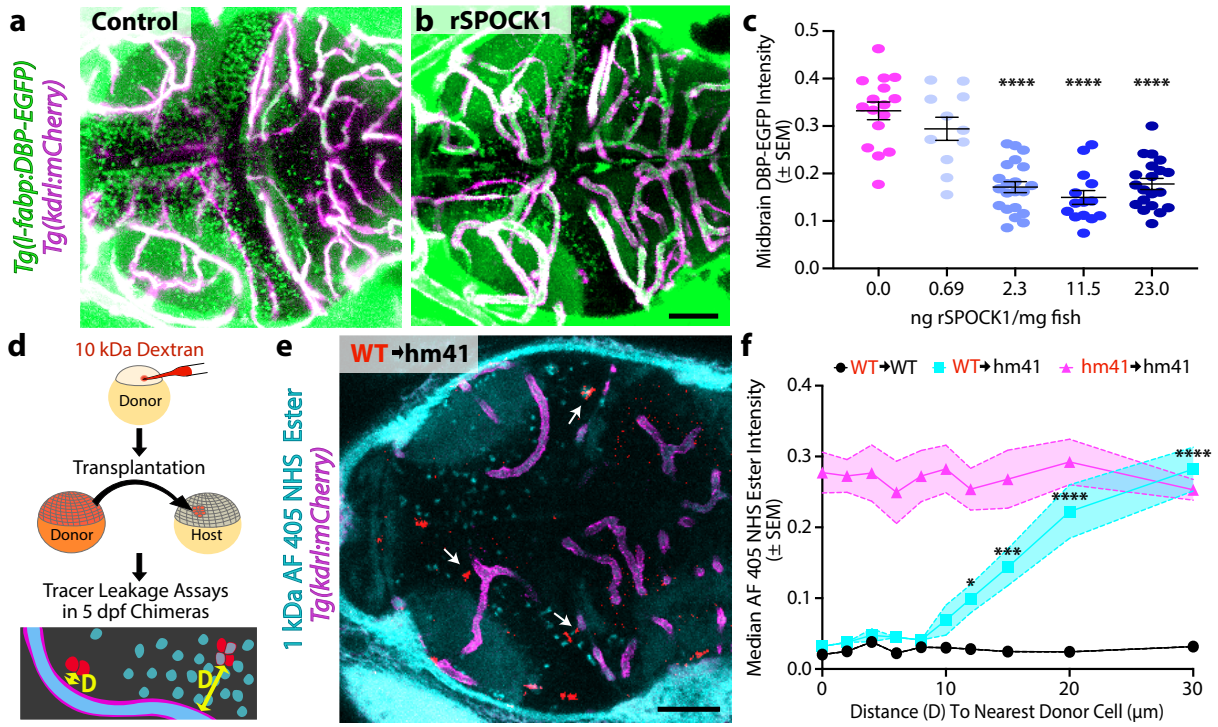

a-b, A single intracranial injection of human rSPOCK1 into the brain at 5 dpf reduces mutant leakage at 6 dpf about 50% (**b**) compared to controls injected with AF 405 NHS Ester alone (**a**). **c**, Quantification of DBP-EGFP in the 6 dpf brain parenchyma after intracranial injection of rSPOCK1. **d**, Schematic of transplantation experiments where donor embryos labeled with 10 kDa Dextran (red) at the single cell stage are transplanted into unlabeled host embryos at sphere stage. Leakage of the injected 1 kDa AF 405 NHS Ester (turquoise) into the midbrain parenchyma is then measured in relationship to the distance (D) from the blood vessel to the nearest donor cell in the 5 dpf chimeric larvae. **e**, Representative dorsal maximum intensity projection image of a chimeric larva with transplanted wild type donor cells (red) into a Spock1$^{hm41/hm41}$ mutant host (WT→hm41). Arrows point to several instances of local rescue of tracer (turquoise) leakage when the wild type donor cells are close but not directly contacting the mutant vasculature (magenta). **f**, Quantification of the NHS leakage in WT→WT (black line) and hm41→hm41 (magenta line) reveals no change in tracer leakage in relationship to the nearest donor cell, with wild type fish confining the tracer and mutant fish leaking the tracer. However WT→hm41 (turquoise line) transplants reveal a full rescue of the leakage in the mutant background when the transplanted cell is within 10 µm of a blood vessel and no effect if the donor cell is further than 20 µm from the vessel. Scale bars represent 50 µm. * p=0.0495, *** p=0.0001, **** p<0.0001 by 2way ANOVA compared to uninjected control mutants in **c** and WT→WT in **f**.

Fig. 3. Spock1 mutants have increased endothelial vesicles.

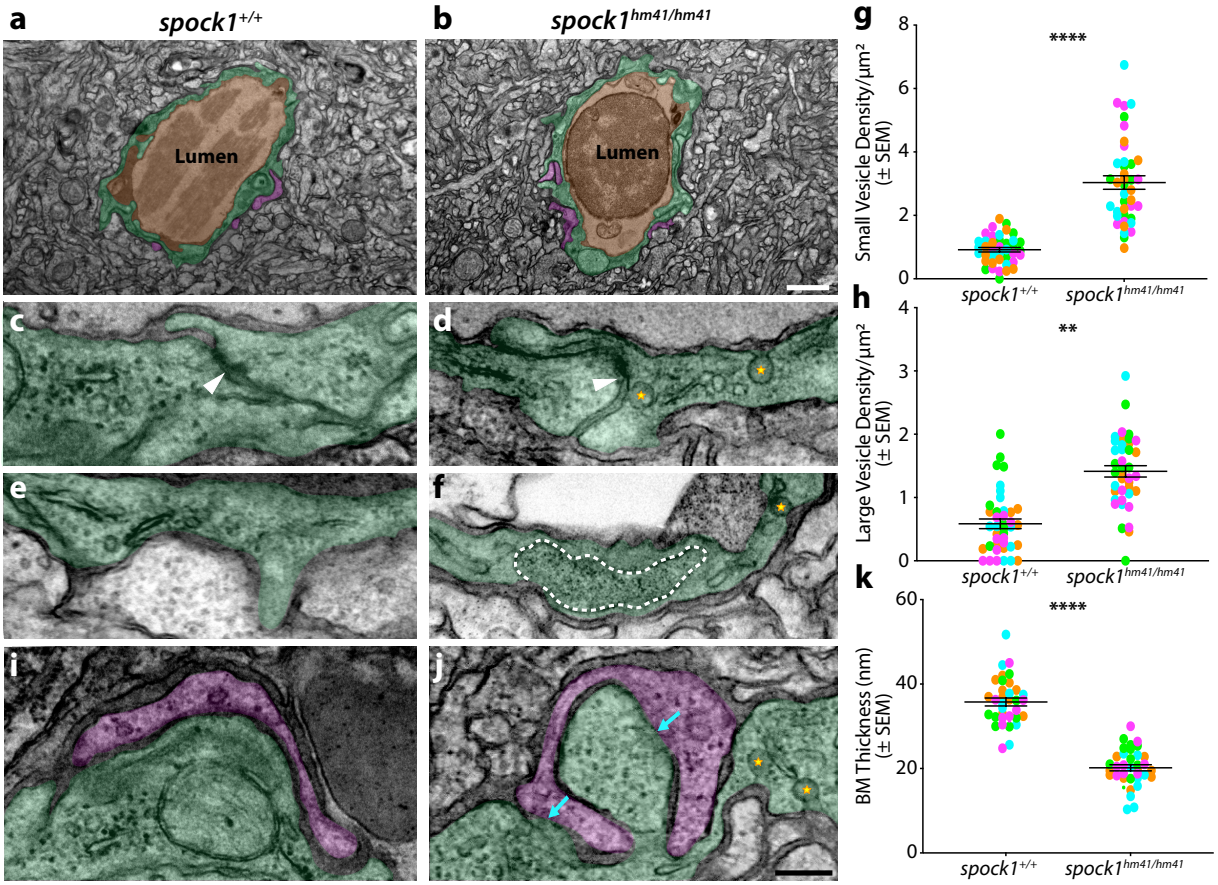

a-b, The neurovascular unit remains intact in *spock1*$^{hm41/hm41}$ mutants (**b**) with a continuous single layer of endothelial cells (pseudocolored green) enclosing the lumen (pseudocolored orange) and in close contact with pericytes (pseudocolored purple). **c-h**, The majority of tight junctions (white arrowheads) are functionally restrictive in the *spock1*^{hm41} mutant endothelial cells (88%). Mutant endothelial cells displayed a significant increase in vesicular density, including both small flask shaped vesicles (yellow stars, **g**) and larger vesicles greater than 200 nm in diameter (outlined by white dashed line in **f**, **h**). **i-k,** While pericyte coverage is unaltered in *spock1*^{hm41} mutants, the pericyte-endothelial cell interactions are altered in the mutants, with several instances of direct pericyte-endothelial cell contact (turquoise arrows) and overall diminished basement membrane thickness (**k**). Scale bars represent 1 µm (**b**) and 200 nm (**j**). N=4 fish, each marked by a unique color, with 10 vessels per fish analyzed and depicted as individual points. ** p=0.0029, **** p<0.0001 by nested t test.

Fig. 4. *Spock1*$^{hm41/hm41}$ mutant vasculature have reduced expression of BBB regulators.

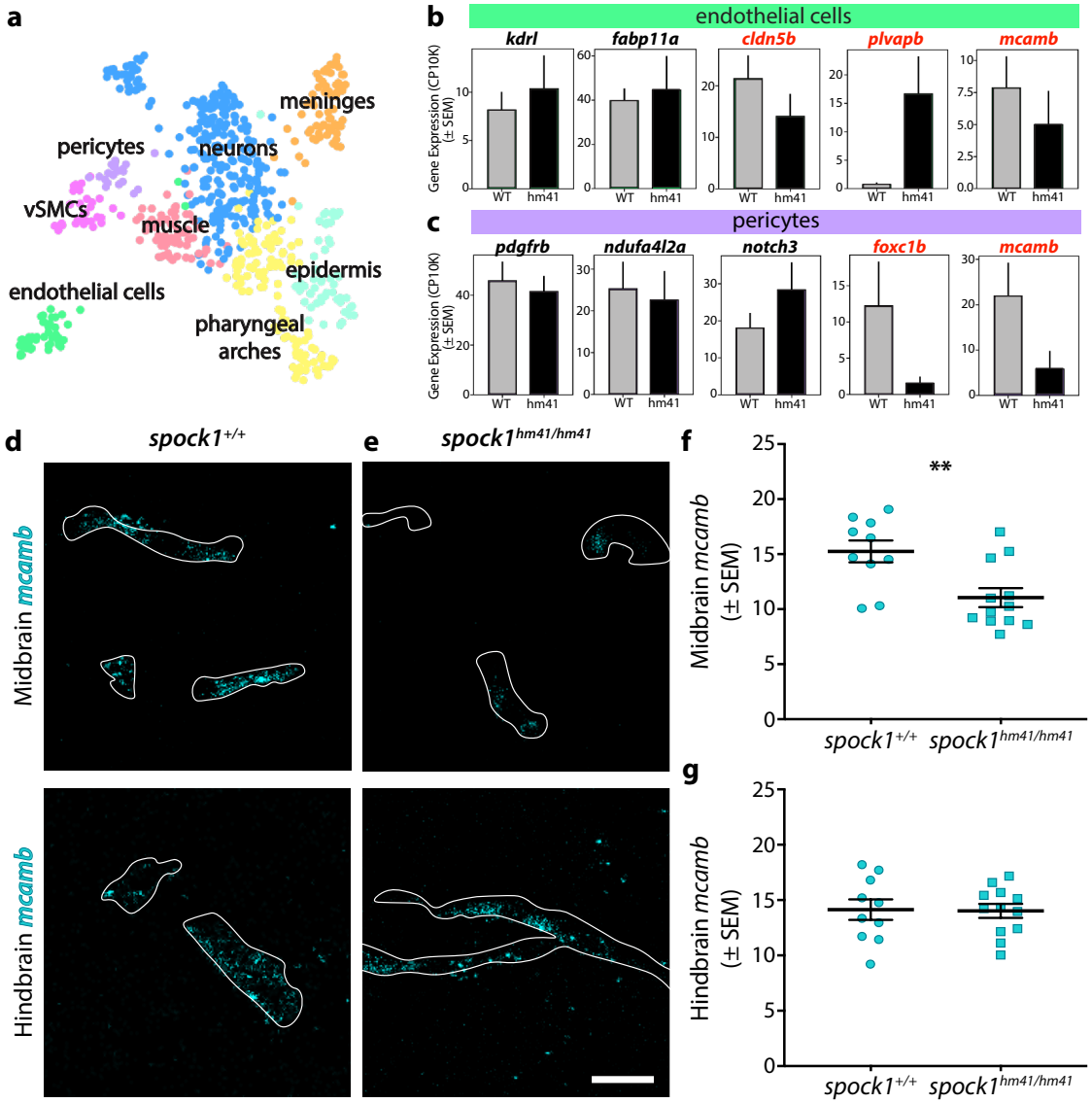

a, UMAP of the subclustered vascular cells separated by cell type, with pericytes (purple) separating from vascular smooth muscle cells (vSMCs, pink) and endothelial cells (green). **b-c**, Mean gene expression in wild type (WT, grey bars) and *spock1* mutant (hm41, black bars) endothelial cells (**b**) and pericytes (**c**). Error bars represent SEM. Mutants appear to have lower levels of *mcamb* in both pericytes and endothelial cells. **d-g**, HCR FISH reveals strong expression of *mcamb* (turquoise) in wild type vasculature (**d**), both in the midbrain and hindbrain. *Spock1* mutants have significantly reduced expression of *mcamb* in the midbrain (**e**, **f**), but normal levels in the hindbrain (**g**), where no leakage is observed. Scale bar represents 10 µm. ** p=0.0044 by unpaired t test.

Materials and Methods

Zebrafish Strains and Maintenance

Zebrafish were maintained at 28.5°C following standard protocols[29]. All zebrafish work was approved by the Harvard Medical Area Standing Committee on Animals under protocol number IS00001263-3. Adult fish were maintained on a standard light-dark cycle from 8 am to 11 pm. Adult fish, age 3 months to 2 years, were crossed to produce embryos and larvae. For imaging live larvae, 0.003% phenylthiourea (PTU) was used beginning at 1 dpf to inhibit melanin production. These studies used the AB wild-type strains and the transgenic reporter strains Tg(*l-fabp:DBP-EGFP)*^{lri500} [16], (Tg(*kdrl:HRAS-mCherry*)^{s896} [30], abbreviated as Tg(*kdrl:mCherry*) in the text, TgBAC(*pdgfrb:EGFP)*^{ncv22Tg} [31], abbreviated as Tg(*pdgfrb:EGFP*).

Spock1^{hm41} Mutants

Spock1^{hm41} mutants were maintained in the double transgenic Tg(*l-fabp:DBP-EGFP; kdrl:mCherry)* background. Heterozygous fish were intercrossed for all leakage assays, with the exception of the time lapse microscopy experiments, where a heterozygous fish was crossed to a homozygous mutant, and the cell transplantation experiments, where homozygous mutants were in-crossed. All larvae were imaged prior to genotyping to identify wild type and mutant fish. The *spock1*^{T241A} mutant line was genotyped using 5'- ACTGAGTGTTATTTTGTCATTGTGC-3' and 5'-TGATGCTGATCTGAGAAGTTTAGCC-3' primers followed by a HaeIII restriction digest, which does not digest the wild-type product (327 bp).

Fluorescent Zebrafish Tracer Injections

Larvae were immobilized with tricaine and placed in an agarose injection mold with their hearts facing upwards. 2.3 nl of Alexa Fluor 405 NHS Ester (Thermo Fisher: A30000) or Alexa Fluor 647 10 kDa Dextran (Thermo Fisher: D22914) fluorescently conjugated tracers (10 mg/ml) were injected into the cardiac sac using Nanoject II (Drummond Scientific, Broomall, PA). Larvae were then mounted with 1.5% low gelling agarose (Sigma: A9414) in embryo water on 0.17 mm coverslips and imaged live within 2 hours post injection on a Leica SP8 laser scanning confocal microscope using the same acquisition settings with 1 µm z-steps using a 25x water immersion objective. All quantification was performed on blinded image sets. For static images, parenchymal fluorescent tracer intensity was measured using ImageJ in the entire regional parenchyma outside of the vasculature in 60 µm thick maximum intensity projections of the larval brains. These projections began on average 15 µm below the mesencephalic vein to reduce the effects of potential leakage diffusion from the surface vessels and had the vasculature masked and removed for intensity quantification. These parenchymal tracer intensity values were then background subtracted and normalized to the tracer intensity within the vasculature to account for differential amounts of circulating tracer between fish. For time lapse imaging, Dextran intensity was measured in six parenchymal regions of average intensity projections of the time lapse videos and averaged as a single value per fish and similarly normalized to the average blood vessel luminal fluorescence intensity at each time point.

Linkage Mapping

Larvae from 2 separate crosses were screened for leakage of DBP-EGFP at 5 dpf and pooled into 3 groups of 5 to 6 leaky or wild type heads. RNA was extracted from the pools using RNeasy mini kit and ribo-depleted. RNA sequencing libraries were prepared using Wafergen Directional RNA-Seq kits and sequenced on NextSeq High-Output sequencers producing 75 bp paired end reads. Reads were mapped to the GRCz11 genome using tophat and bowtie2. Linkage mapping was performed on the mapped reads using RNAmapper[17] with the following specifications: zygosity=25, coverage=1, linkedRatio=0.96, neighbors=10. Differential gene expression analysis was performed on these libraries using rsem[32].

334
335 **CRISPR Mutants**
336 *Gstp2* crispant fish were generated by injection of Cas9 protein and 3 guide RNAs (5'-
337 CAGCTGCCTAAATTTGAAGA-3', 5'-GCGTTGGAAACTTACACATG-3', and 5'-GTGAGAGTGT
338 AGGGAGCCAC-3') into 1-cell fertilized double transgenic Tg(*l-fabp:DBP-EGFP; kdrl:mCherry)*
339 embryos. *Csf1ra* crispant fish were generated similarly with 4 guide RNAs (5'-
340 CTGCTCACCAACAGCCGAG-3', 5'-GTGTCTTCTGACCGACCCGG-3', 5'-CTCGTCTTCATGCT
341 TCACG-3', and 5'-AGTGACACCTTCTCCATGG-3'), as were *spock1* crispants (5'-GTAGCCGAC
342 AGAAAGAGAGG-3', 5'-GAGTCGCAGGAGTTGAACAG-3', 5'-GACAGTGAACCTTCATGCAG-
343 3', and 5'-TGTCCGGGCAGGCAAGGGCA-3'). F0 crispants were analyzed for leakage of the
344 DBP-EGFP tracer outside of the kdrl:mCherry labeled vasculature at 5 dpf.
345
346 **HCR Fluorescent In Situ Hybridization (FISH)**
347 HCR RNA in situ hybridization (Molecular Instruments) experiments on 14 µm cryosections of
348 fixed 5 dpf larvae were performed as previously described[15,33]. Briefly, sections were air dried and
349 re-fixed in 4% paraformaldehyde in PBS for 10 minutes at room temperature. Following fixation,
350 slides were washed in PBS and then permeabilized using 1 µg/ml Proteinase K (ThermoFisher)
351 for 5 minutes, followed by PBS washes and refixation. Tissues were further permeabilized by an
352 ethanol dehydration series of 50%, 70% and two rounds of 100% ethanol and air dried for 5
353 minutes. Dried slides were put into pre-hyb solution for at least 10 minutes at 37°C. Subsequently,
354 the probes for *spock1, kdrl, elavl3,* and *mcamb* were added to the slides at a final concentration
355 of 4 nM to hybridize overnight at 37°C. The next day, slides were washed with a series of wash
356 buffer to 5x SSCT (5x SSC with 0.1% Tween 20). Excess liquid was then removed and samples
357 were immersed in amplification buffer at room temperature for 30 minutes prior to hairpin
358 amplification, which occurred overnight at room temperature. Slides were then washed in 5x
359 SSCT, washed in 5x SSC and mounted with Fluoromount-G (Electron Microscopy Sciences).
360
361 Images were collected on a Leica SP8 laser scanning confocal microscope using the same
362 acquisition settings with 0.2 µm z-steps using a 25x water immersion objective or a 63x oil
363 immersion lens. All quantification was performed on blinded image sets of sections from a single
364 slide treated with all of the same reagents and imaged on the same day. To measure levels of
365 *mcamb* expression, we used ImageJ to first subtract tissue autofluorescence (captured in the 405
366 channel) from the *mcamb* expression in maximum intensity projections and then the vasculature
367 was manually traced and average intensity was measured.
368
369 **Mouse Maintenance**
370 *Spock1*$^{-/-}$ knockout mice were obtained from Ursula Hartmann's lab and were backcrossed to and
371 maintained on a C57Bl/6 background. Mice were genotyped with primers 5'-GCCACTGGTCATT
372 GTCTAGG-3', 5'- TGTGCCCAGTCATAGCCGAATAGCCTCTCC-3', and 5'-GCTTGAGGTAGC
373 CCTGTTGTCACC-3' using KAPA HiFi Hotstart polymerase (Roche:KK2602). This PCR reaction
374 produced a 185 bp wild type band and a 750 bp knockout band in heterozygous animals. All
375 animals were treated according to institutional and US National Institutes of Health (NIH)
376 guidelines approved by the Institutional Animal Care and Use Committee (IACUC) at Harvard
377 Medical School under protocol IS00000045-6.
378
379 **Mouse Embryonic Tracer Injection**
380 Heterozygous *Spock1*$^{+/-}$ mice were intercrossed and used for the tracer leakage assays
381 performed at embryonic day 15.5 (E15.5) as previously described[20]. In brief, 5 µl of tracer cocktail
382 (10 mg/ml EZ-Link NHS-Biotin (Thermo Fisher: 20217) and 10 kDa Dextran Alexa Fluor 488
383 (Thermo Fisher: D22910)) was injected into the liver of each embryo and allowed to circulate for
384 5 minutes. Embryonic heads were fixed by immersion in 4% paraformaldehyde overnight at 4°C

385 and then frozen in TissueTek OCT (Sakura). 20 µm thick sections were then collected and
386 immunostained with Streptavidin Alexa Fluor 405 (1:200; Thermo Fisher: S32351) and rat anti-
387 PLVAP (1:200; BD Biosciences:553849). All embryos were injected blind before genotyping.
388
389 **Transplantation**
390 Donor embryos were injected with 2.3 nl of 10 mg/ml Alexa Fluor 647 10 kDa Dextran (Thermo
391 Fisher: D22914) at the 1-cell stage to distinguish them from host cells. Following injection,
392 embryos were incubated at 28.5°C until transplantation. Host and donor embryos were
393 dechorinated with 1 mg/ml Pronase (Roche:11459643001) at oblong stage and transferred to
394 transplantation agarose dishes in 1/3 Ringer's buffer. Unfertilized or injured embryos were
395 discarded. To generate clonal sources secreting wild type or mutant Spock1, approximately 40–
396 80 cells were transplanted from sphere stage dextran labeled donor embryos into sphere stage
397 wild type and mutant hosts (similar to previous studies[34]). Embryos recovered overnight in 1/3
398 Ringer's buffer and were subsequently transferred to Danieau Buffer with PTU. Tracer injections
399 were performed at 5 dpf, as described above, with 1 kDa Alexa Flour 405 NHS Ester. Blinded
400 image sets were analyzed using ImageJ. Individual larval brains were segmented into 10 µm thick
401 maximum intensity projections spanning the entire brain. Average NHS tracer intensity was
402 measured in 10 µm wide swaths connecting donor cells to the nearest blood vessel and
403 normalized to average blood vessel tracer intensity. The median tracer intensity for a given
404 distance (D) to the nearest donor cell was calculated for each individual fish.
405
406 **Transmission Electron Microscopy (TEM)**
407 Larvae (7 dpf) were anesthetized with tricaine and injected with 2.3 nl of 5 nm NHS-activated gold
408 nanoparticles (Cytodiagnostics: CGN5K-5-1, ~1.1^{14} particles/ml in PBS) just as for the fluorescent
409 tracer injections. After 5 minutes of circulation, the larvae were initially fixed by immersion in 4%
410 paraformaldehyde (VWR:15713-S) /0.1M sodium-cacodylate (VWR:11653). Following this initial
411 fixation, larvae were further fixed for 7 days in 2% glutaraldehyde (Electron Microscopy Sciences:
412 16320)/ 4% paraformaldehyde/ 0.1M sodium-cacodylate at room temperature. Following fixation,
413 larvae were washed overnight in 0.1M sodium-cacodylate. Entire larval heads were post-fixed in
414 1% osmium tetroxide and 1.5% potassium ferrocyanide, dehydrated, and embedded in epoxy
415 resin. Ultrathin sections of 80 nm were then cut from the block surface and collected on copper
416 grids. Grids were imaged using a 1200EX electron microscope (JEOL) equipped with a 2k CCD
417 digital camera (AMT) and quantified using ImageJ (NIH). Vesicular density values were
418 calculated from the number of non-clathrin coated small vesicles less than 100 nm in diameter or
419 large vesicles greater than 200 nm in diameter per μm^2 of endothelial area for each image
420 collected. Average pericyte basement membrane (BM) thickness was quantified by measuring
421 the total BM area divided by the length of the pericyte-endothelial contact. All images for analysis
422 were collected at 12000x magnification. 10-15 vessels were quantified for each fish, with each
423 color representing a different fish.
424
425 **Single-cell RNA-sequencing**
426
427 Larval zebrafish brains were dissected and split along the midbrain-hindbrain boundary in DMEM.
428 Brains were dissociated using a modified protocol[35]. Briefly, chemical dissociations were
429 performed at 30.5°C using a mixture of 0.25% Trypsin-EDTA, Collagenase/Dispase (8 mg/mL)
430 and DNaseI (20 µg/mL) for 15-20 minutes with gentle pipetting every few minutes and quenched
431 with 10% fetal bovine serum in DMEM. Samples were hashed using Multi-seq as previously
432 described with slight modifications[36]. For each sample, 80 pmoles of lipid modified oligos (LMOs)
433 were used to hash every 500k cells. The hashing reaction was quenched using 1% BSA in PBS
434 and barcoded samples were subsequently pooled and washed with 1% BSA. The pooled cell
435 mixture was resuspended in PBS + 0.1%BSA + 18% Optiprep at a final concentration of ~300k

436 cells/mL prior to single-cell capture with inDrops. The Single-cell Core (SCC) at Harvard Medical
437 School captured single-cell transcriptomes and prepared NGS libraries as previously described[37]
438 with a target capture of 45k cells per experiment. A summary of dissected tissues and
439 corresponding sequencing information are described in Table S4.
440
441 Gene expression and hashtag libraries were mixed (9:1 ratio) and sequenced on an Illumina
442 Nova-seq 6000 with the NovaSeq S2 kit. Reads were mapped onto the Zebrafish GRCz11
443 Release 101 genome assembly using previously described methods[38]. Hashtags were identified
444 using custom code available on: https://github.com/AllonKleinLab/paper-
445 data/tree/master/OBrown2021_ZebrafishBBB
446
447 Transcriptomes with greater than 350 UMIs were further filtered for viability by removing cells with
448 >20% mitochondrial reads. Cell demultiplexing was performed manually by applying thresholds
449 to delineate single cells from background and multiple populations. The resulting counts matrix
450 was normalized to the mean UMIs per cell in the dataset.
451
452 To visualize the data, we first mean-normalized the data and identified highly variable genes from
453 the wild type AB and RNF datasets (minimum of 3 transcripts per cell, minimum of 3 cells
454 expressing gene, minimum V-score percentile of 85%). We then Z-scored counts for each gene
455 and performed principal component analysis (PCA) with 50 components. Cells from the spock1
456 mutant libraries were projected into the same principal component subspace. A k-nearest
457 neighbor graph (k=10) was generated based on the Euclidean distance in gene expression
458 between cells within this subspace. The Leiden algorithm was used to cluster cells into
459 subgroups[39]. The neighborhood graph was embedded and visualized using UMAP and the data
460 was explored interactively with SPRING[40] to aid in cell cluster annotation.
461
462 Cells belonging to the liver, pharyngeal arches, skin, and muscle were removed prior to differential
463 gene expression (DGE) analysis. The filtered dataset was reanalyzed using the methods
464 described above. The Wilcoxon rank-sum test was used to generate a list of potential genes that
465 are differentially regulated (fold change > 2) between genotypes across each Leiden cluster
466 (Table S2). Genes were only considered for DGE analysis if they were expressed in at least 5%
467 of cells in a given cluster and had a minimum mean of 10 transcripts per cell. Cells belonging to
468 the AB and RNF background were treated as a single wild type genotype for the analysis. The
469 vascular cluster (Leiden 13) was subclustered and similarly analyzed for DGE (Table S3).
470
471 **Data availability**
472
473 The raw reads from the counts matrix and associated metadata from the single-cell experiments
474 have been deposited to GEO. (Accession #)
475
476 All code for the single-cell analysis is available as interactive Jupyter notebooks here:
477 https://github.com/AllonKleinLab/paper-data/tree/master/OBrown2021_ZebrafishBBB
478
479 Interactive exploration of the full single-cell data can be found here:
480 https://kleintools.hms.harvard.edu/tools/springViewer_1_6_dev.html?client_datasets/2021_OBr
481 own/2021_OBrown
482
483 Exploration of the vascular subcluster cells can be found here:
484 https://kleintools.hms.harvard.edu/tools/springViewer_1_6_dev.html?client_datasets/2021_OBr
485 own_Vasculature/2021_OBrown_Vasculature

Supplemental Figures

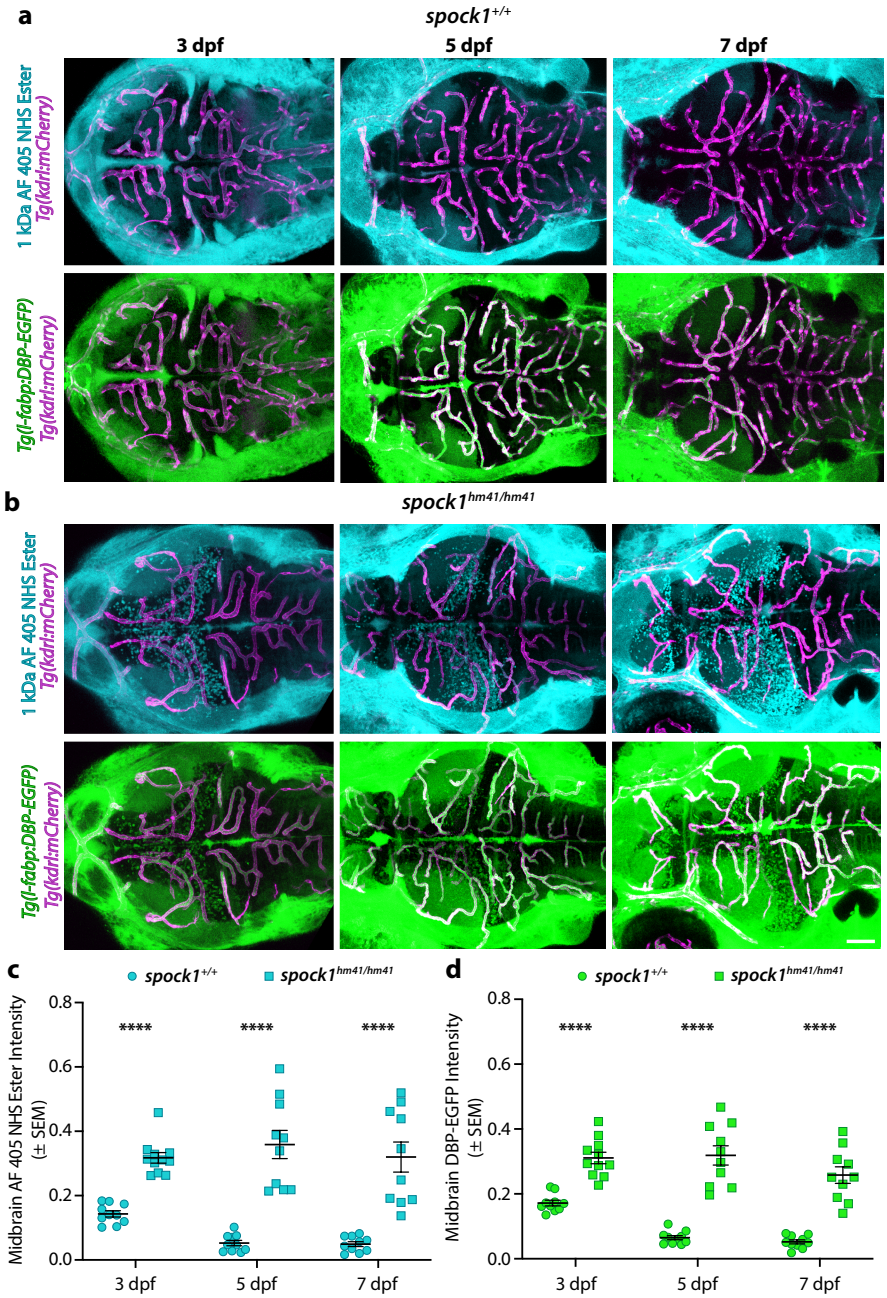

Extended Data Fig. 1. *Spock1*$^{hm41/hm41}$ mutants display increased BBB permeability as early as 3 dpf and maintain this leakage throughout larval development. a, Developmental time series of injected 1 kDa AF 405 NHS Ester (turquoise) and transgenic 80 kDa DBP-EGFP (green) serum protein tracer in wild type fish reveals a functional sealing of the BBB by 5 dpf, as previously observed.[15] b, *Spock1*$^{hm41/hm41}$ mutants leak both injected 1 kDa AF 405 NHS Ester and the transgenic 80 kDa DBP-EGFP serum protein as early as 3 dpf, in the forebrain and midbrain. This leakage pattern and intensity is maintained at 5 and 7 dpf. c-d, Quantification of AF 405 NHS Ester (c) and DBP-EGFP (d) in the midbrain parenchyma outside of the vasculature. Scale bar represents 100 µm. **** $p<0.0001$ by 2way ANOVA compared to wild type controls.

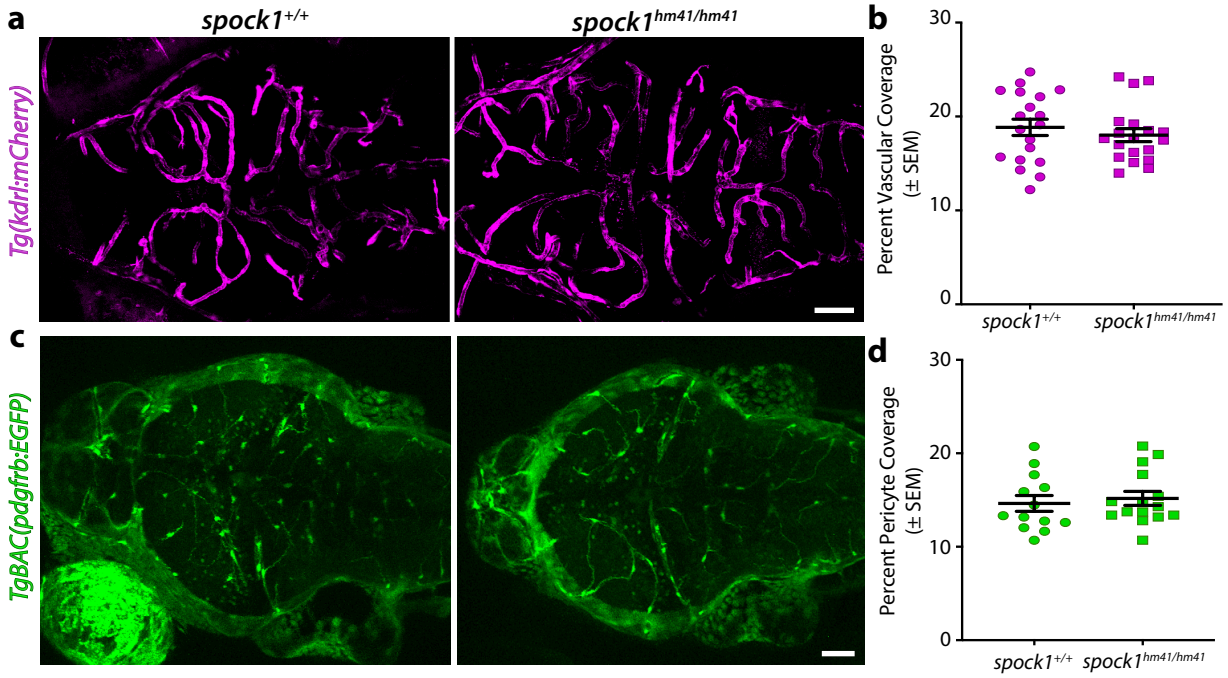

Extended Data Fig. 2. *Spock1*$^{hm41/hm41}$ mutants display normal vascular and pericyte coverage of the brain. a, Dorsal maximum intensity projection of wild type (left) and mutant (right) brains with endothelial cells marked by the kdrl:mCherry transgene (magenta). **b**, Quantification of total vascular coverage of the brain as (kdrl:mCherry+ area/total brain area), with each individual fish marked by a single point. **c**, Top down maximum intensity projection of wild type (left) and mutant (right) brains with pericytes marked by the pdgfrb:EGFP transgene (green). **d**, Quantification of total pericyte coverage of the vasculature (pdgfrb:EGFP+ area/kdrl:mCherry+ area), with each individual fish marked by a single point. T-test comparison reveals no significant difference between wild type and mutant fish for either vascular or pericyte coverage. Scale bars represent 50 μm.

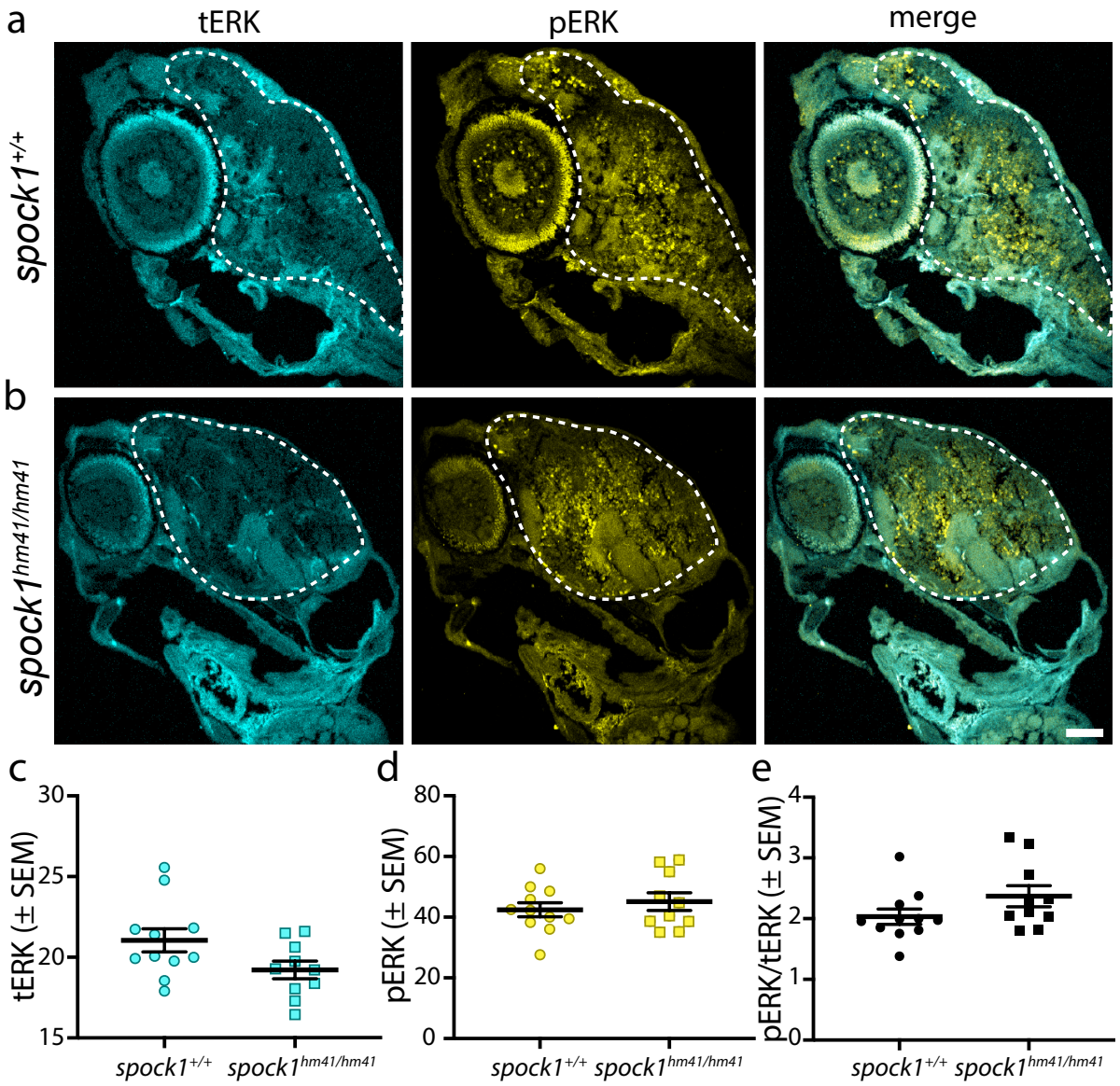

Extended Data Fig. 3. Neuronal activity is unaltered in *spock1* mutants. a-b, Immunostaining for total ERK (tERK) and phosphorylated ERK (pERK) reveals no change in neuronal activity in *spock1* mutants (**b**) compared to wild type siblings (**a**). Brains are outlined by white dashed lines. **c-e**, Quantification of tERK (**c**), pERK (**d**) and the ratio of pERK/tERK (**e**) as a readout of neural activity with each individual fish marked by a single point. Scale bar represents 100 μm.

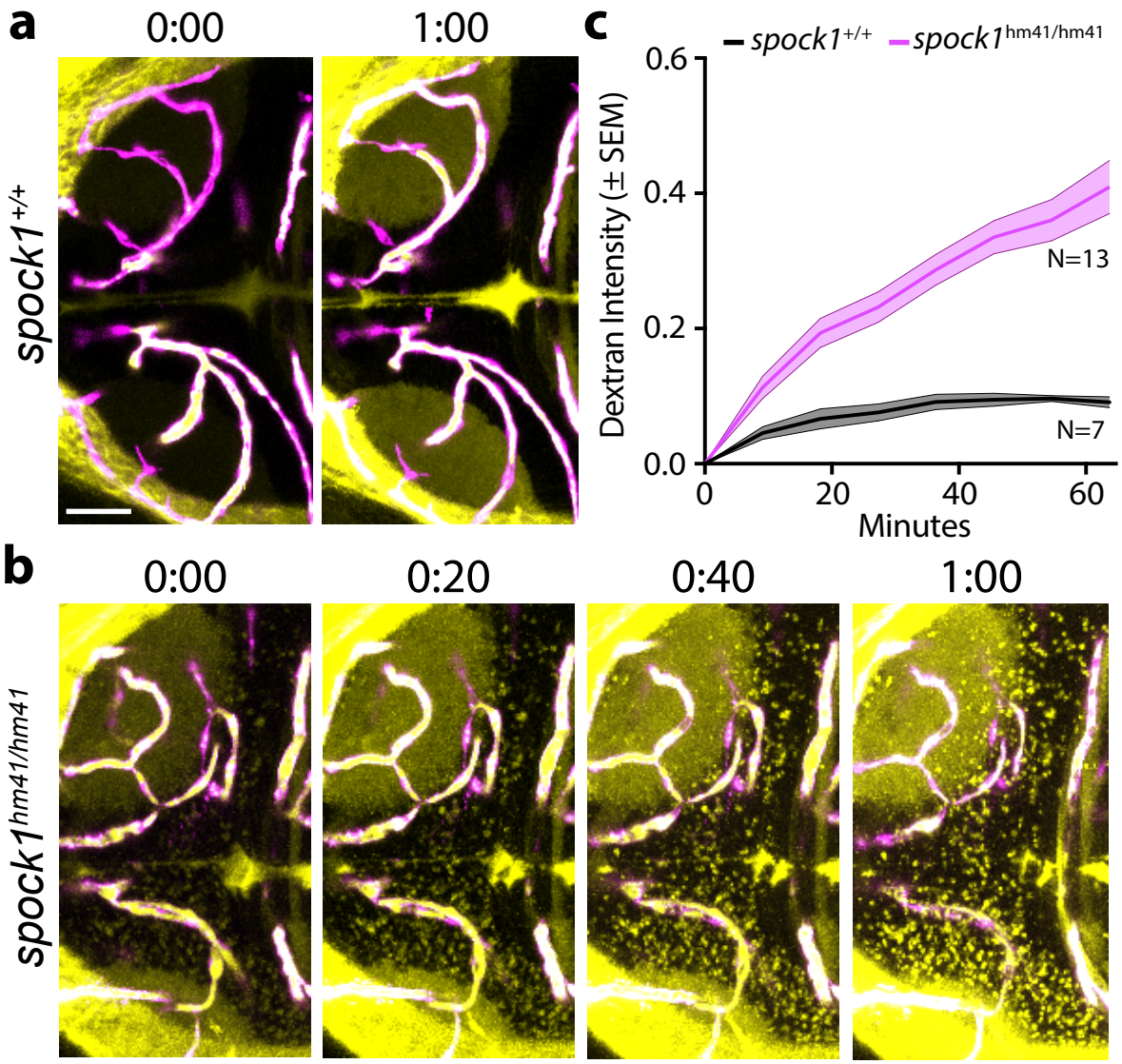

514
515 **Extended Data Fig. 4. Time lapse imaging reveals leakage dynamics in *spock1*$^{hm41/hm41}$**
516 **mutants.** **a-b**, Dorsal maximum intensity projection of a wild type (**a**) and *spock1*$^{hm41/hm41}$ mutant
517 (**b**) midbrain reveals steady accumulation of 10 kDa Dextran (yellow) outside of the vasculature
518 (magenta) over the course of one hour in *spock1* mutants. **c**, Quantification of Dextran
519 accumulation in the midbrain parenchyma outside of the vasculature over time in wild type fish
520 (black line) and *spock1*$^{hm41/hm41}$ mutants (magenta line). Scale bar represents 50 µm.

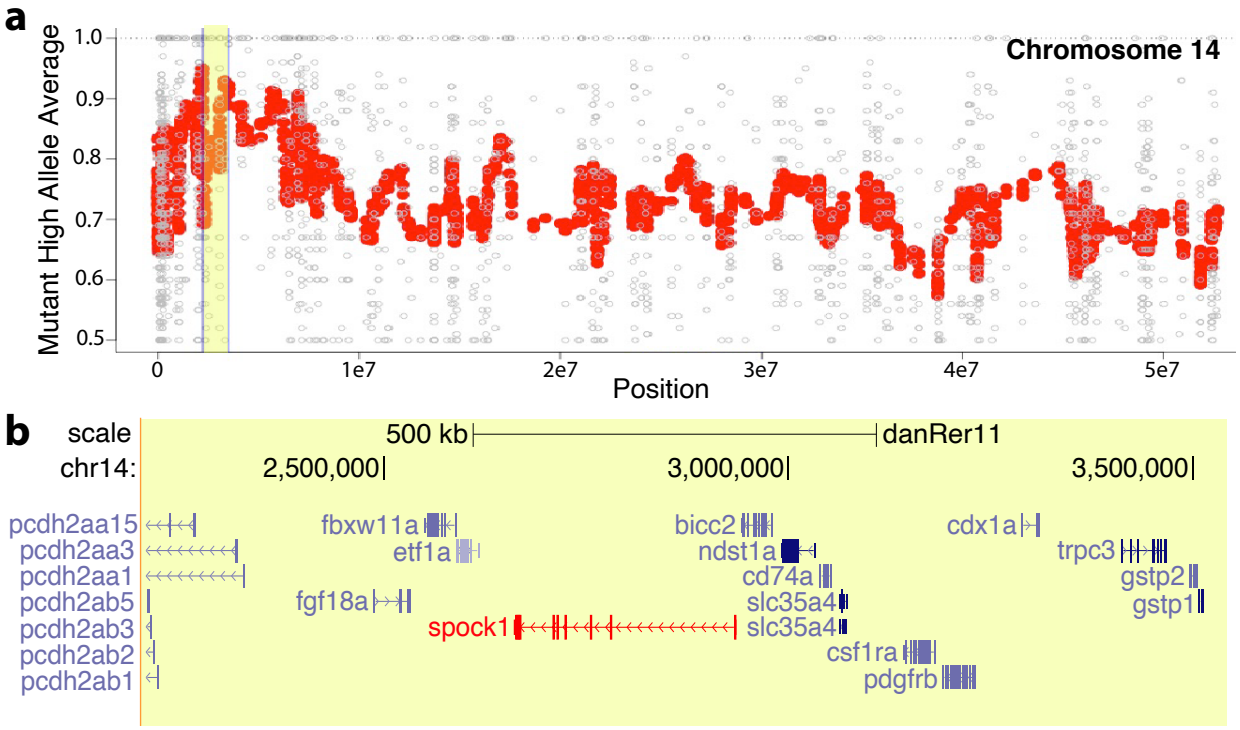

Extended Data Fig. 5. Leaky phenotype maps to chr14:2205271-3513919. a, Manhattan plot of linkage on chromosome 14 with the average mutant alleles per 20 neighbors plotted in red. The region of highest linkage is highlighted in yellow. **b**, Genome browser view of the highest linked region to the leaky phenotype. Eight of the genes within this region were expressed in the 5 dpf bulk RNAseq data: *fgf18a, spock1, bicc2, csf1ra, ndst1a, slc35a4, gstp1* and *gstp2*. Two of these genes were differentially expressed in leaky mutants compared to wild type (*csf1ra* and *gstp2*) and *spock1* (marked in red) had several SNPs that completely segregated in the leaky fish.

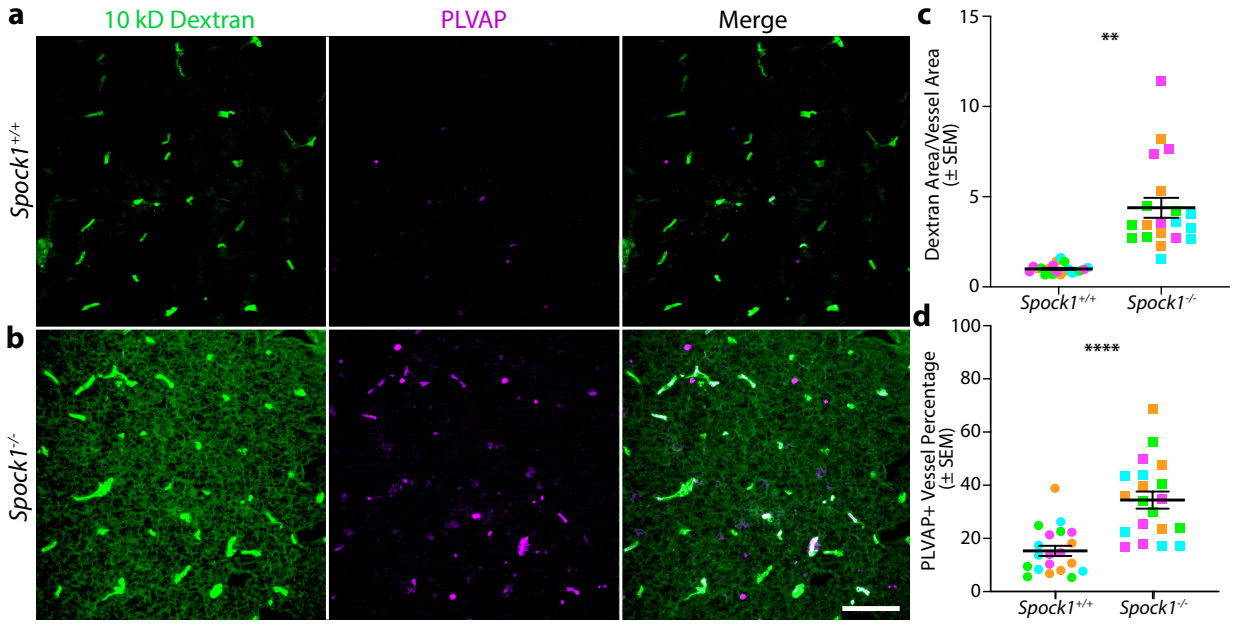

Extended Data Fig. 6. Increased *Spock1*$^{-/-}$ leakage of 10 kDa Dextran is associated with an increase in PLVAP expression. a-b, Zoomed in view of 10 kDa Dextran (green) confined within the vasculature of wild type (**a**) vessels and leaked out into the cortex of *Spock1*$^{-/-}$ knockouts (**b**). This increased BBB permeability in *Spock1*$^{-/-}$ mice is accompanied by an increase in PLVAP (magenta) expression in the vasculature. **c**, Quantification of the total area of Dextran leakage normalized to vessel area where a ratio of 1 indicates no leakage reveals a significant increase in Dextran extravasation in the *Spock1*$^{-/-}$ embryos (p=0.0048 by nested t test). **d**, Quantification of PLVAP expression within the vasculature reveals a significant increase in PLVAP expression in the *Spock1*$^{-/-}$ embryos (p<0.0001 by nested t test). N=4 embryos for each genotype, marked by unique colors, with 5 sections analyzed per embryo. Scale bar represents 50 µm.

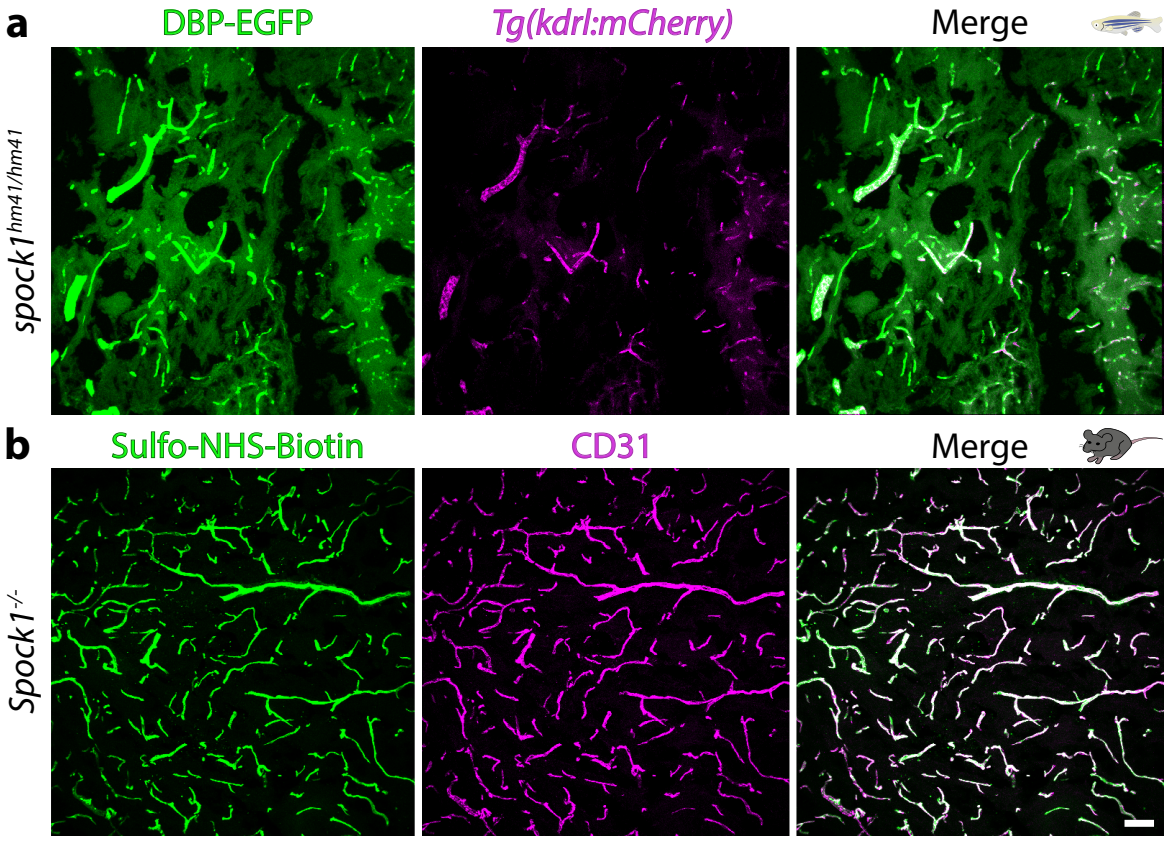

Extended Data Fig. 7. *Spock1*$^{-/-}$ mice recover BBB function in adulthood but *spock1*$^{hm41/hm41}$ mutant fish remain leaky. a, Zoomed in section of an adult zebrafish *spock1*$^{hm41/hm41}$ brain reveals continued leakage of the transgenic serum tracer DBP-EGFP (green) outside of the vasculature (magenta). **b**, Adult *Spock1*$^{-/-}$ knockout mice, on the other hand, confine the injected Sulfo-NHS-Biotin tracer (green) within the CD31+ vasculature (magenta), indicating a functional BBB. Scale bar represents 50 µm.

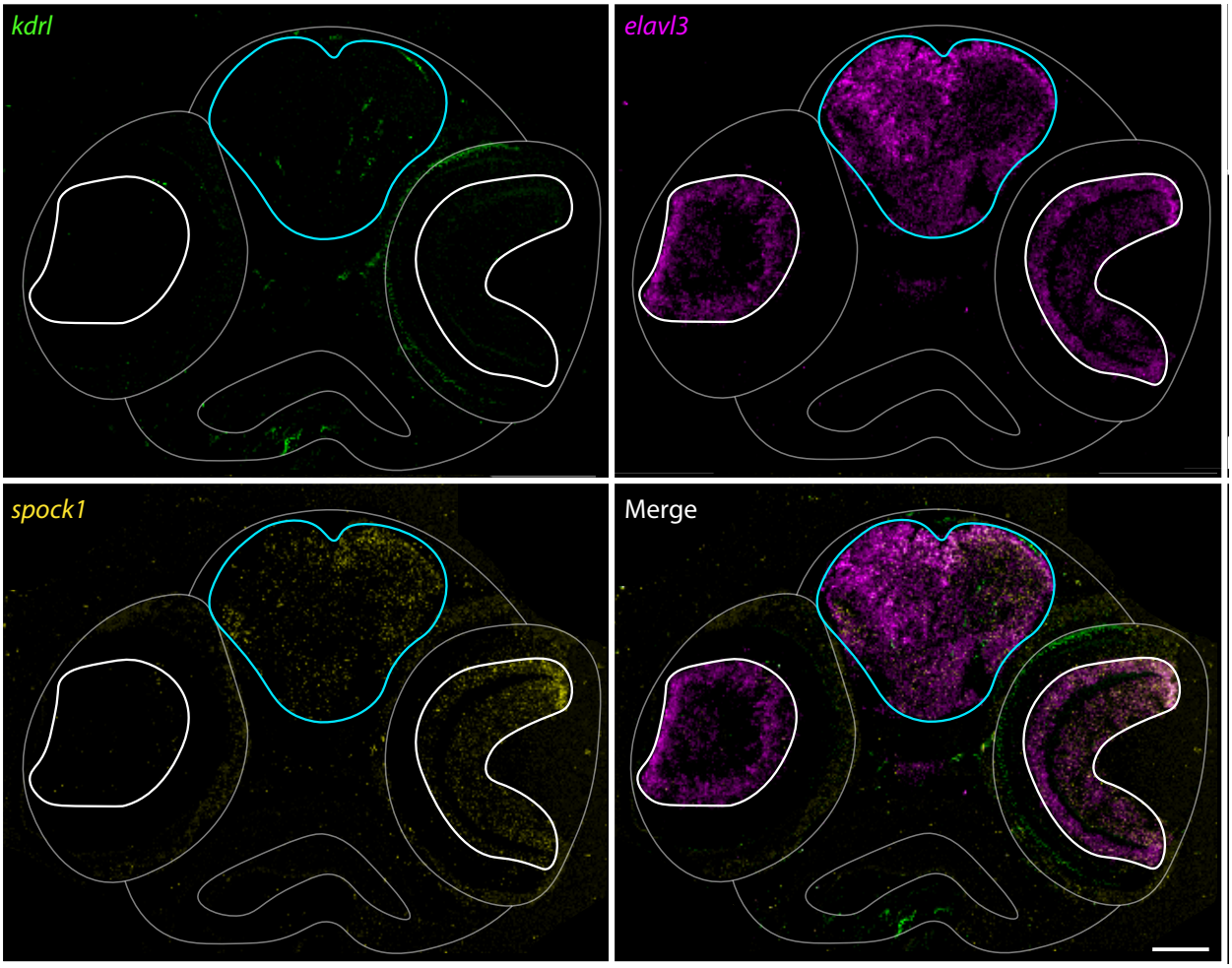

Extended Data Fig. 8. *Spock1* is expressed throughout the developing central nervous system. *Spock1* expression (yellow) colocalizes with neuronal *elavl3* (magenta) expression in the brain (outlined in turquoise) and retina (both outlined in white) of the 4 dpf fish but not the vascular *kdrl* signal (green). Scale bar represents 50 μm.

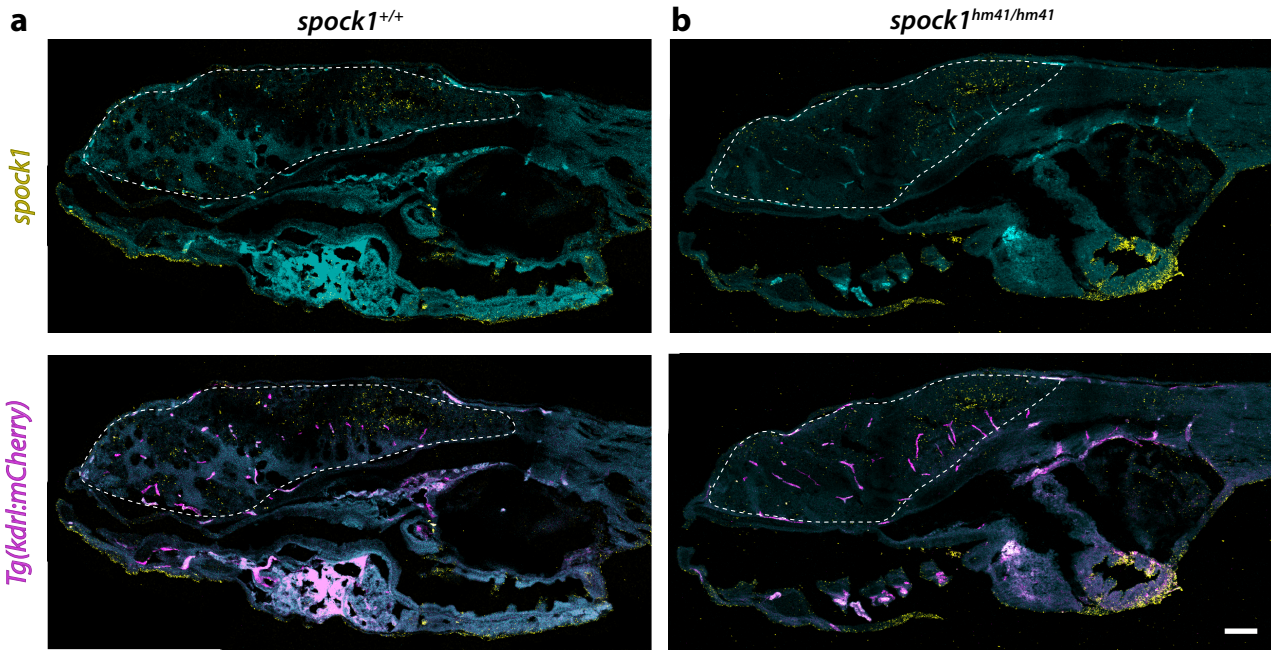

555
556 **Extended Data Fig. 9. Expression of *spock1* is unaltered in *spock1*$^{hm41/hm41}$ mutants. a-b,**
557 *Spock1* expression (yellow) is found throughout the brain and spinal cord (outlined by a white
558 dashed line) in wild type (**a**) and *spock1*$^{hm41/hm41}$ mutant fish (**b**) at 5 dpf. *Spock1* expression never
559 colocalizes with vascular *Tg(kdrl:mCherry)* expression (magenta). Tissue autofluorescence is
560 depicted in turquoise. Scale bar represents 50 μm.

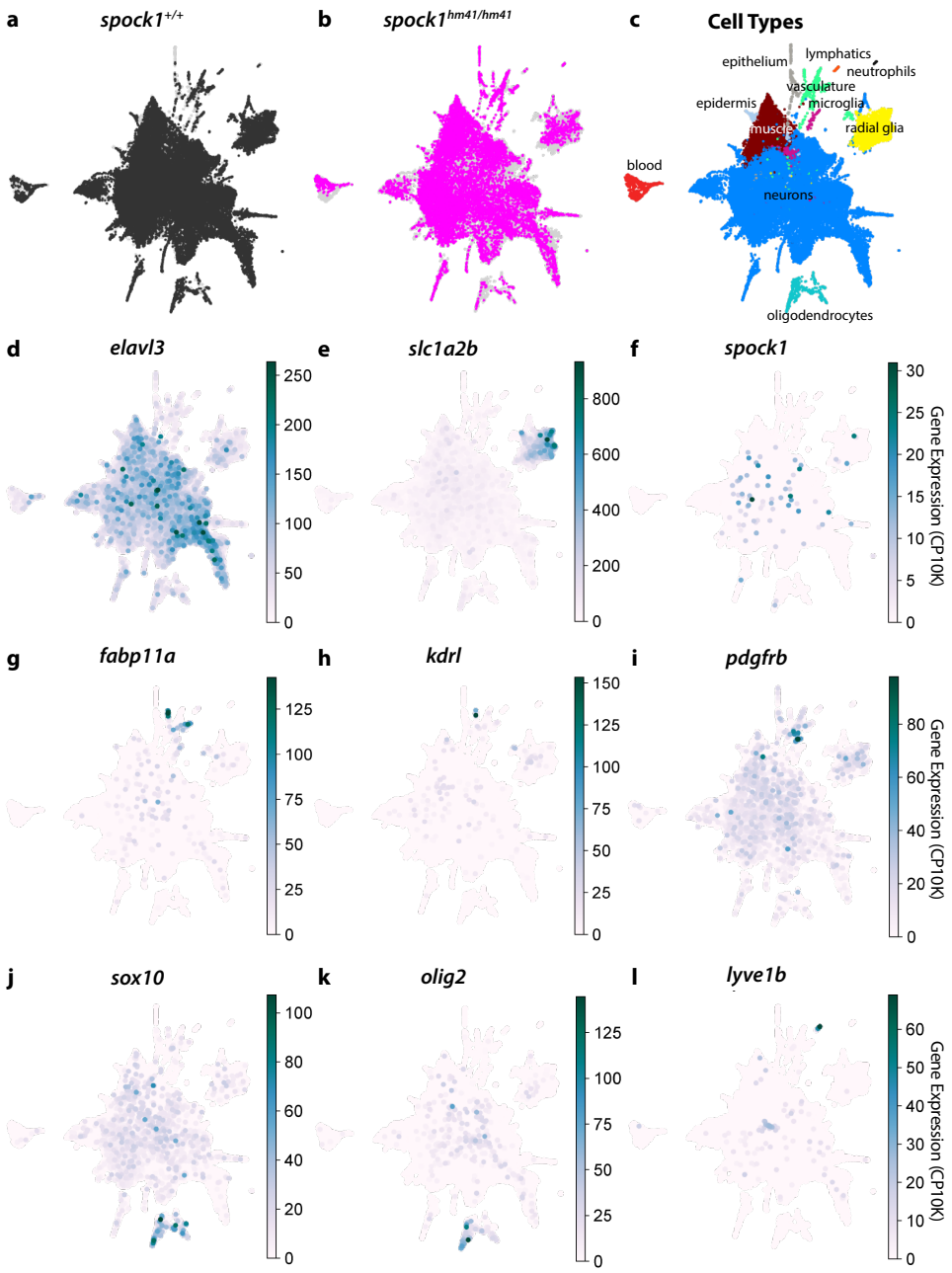

Extended Data Fig. 10. scRNA-seq captures all neurovascular cells in both mutant and wild type larvae. a-b, UMAP of the whole brain dataset separated shows overlap between wild type (**a**) and *spock1*$^{hm41/hm41}$ mutant (**b**) cell type coverage, indicating that no cell type is absent in the mutant background. **c**, UMAP of the total data set separated by annotated cell type, with the vast majority of sequenced cells being neuronal (blue). Our data does capture blood cells (red), microglia (magenta), oligodendrocytes (aqua), radial glia (yellow), and vascular cells (green). **d-l**, Gene expression plots for *elavl3* (**d**) for neurons, *slc1a2b* (**e**) for radial glia, *fabp11a* (**g**) and *kdrl* (**h**) for endothelial cells, *pdgfrb* (**i**) for pericytes and neurons, *sox10* (**j**) and *olig2* (**k**) for oligodendrocytes, and *lyve1b* (**l**) for lymphatic endothelial cells reveals that *spock1* (**f**) is primarily expressed by neurons and absent from the vascular cells.

572 References

573 1. Sweeney, M. D., Sagare, A. P. & Zlokovic, B. V. Blood–brain barrier breakdown in Alzheimer
574 disease and other neurodegenerative disorders. *Nature Publishing Group* 14, 133–150 (2018).

575 2. Reese, T. S. & Karnovsky, M. J. Fine structural localization of a blood-brain barrier to
576 exogenous peroxidase. *J Cell Biology* 34, 207–217 (1967).

577 3. Stewart, P. A. & Wiley, M. J. Developing nervous tissue induces formation of blood-brain
578 barrier characteristics in invading endothelial cells: A study using quail-chick transplantation
579 chimeras. *Dev Biol* 84, 183–192 (1981).

580 4. Lyck, R. *et al.* Culture-induced changes in blood-brain barrier transcriptome: implications for
581 amino-acid transporters in vivo. *Journal of cerebral blood flow and metabolism : official journal*
582 *of the International Society of Cerebral Blood Flow and Metabolism* 29, 1491–1502 (2009).

583 5. Urich, E., Lazic, S. E., Molnos, J., Wells, I. & Freskgård, P.-O. Transcriptional Profiling of
584 Human Brain Endothelial Cells Reveals Key Properties Crucial for Predictive In Vitro Blood-
585 Brain Barrier Models. *PloS one* 7, e38149-16 (2012).

586 6. Heithoff, B. P. *et al.* Astrocytes are necessary for blood-brain barrier maintenance in the adult
587 mouse brain. 99, 125–70 (2020).

588 7. Guérit, S. *et al.* Astrocyte-derived Wnt growth factors are required for endothelial blood-brain
589 barrier maintenance. *Prog Neurobiol* 199, 101937 (2021).

590 8. Daneman, R. *et al.* Wnt/beta-catenin signaling is required for CNS, but not non-CNS,
591 angiogenesis. *Proceedings of the National Academy of Sciences of the United States of*
592 *America* 106, 641–646 (2009).

593 9. Guérit, S. *et al.* Astrocyte-derived Wnt growth factors are required for endothelial blood-brain
594 barrier maintenance. *Progress in Neurobiology* 334, 101937–19 (2020).

595 10. Benz, F. *et al.* Low wnt/β-catenin signaling determines leaky vessels in the subfornical organ
596 and affects water homeostasis in mice. *Elife* 8, e43818 (2019).

597 11. Stenman, J. M. *et al.* Canonical Wnt Signaling Regulates Organ-Specific Assembly and
598 Differentiation of CNS Vasculature. *Science* 322, 1247–1250 (2008).

599 12. Wang, Y. *et al.* Norrin/Frizzled4 signaling in retinal vascular development and blood brain
600 barrier plasticity. *Cell* 151, 1332–1344 (2012).

601 13. Vanhollebeke, B. *et al.* Tip cell-specific requirement for an atypical Gpr124- and Reck-
602 dependent Wnt/β-catenin pathway during brain angiogenesis. *eLife* 4, (2015).

603 14. Wang, Y. *et al.* Interplay of the Norrin and Wnt7a/Wnt7b signaling systems in blood–brain
604 barrier and blood–retina barrier development and maintenance. *Proceedings of the National*
605 *Academy of Sciences of the United States of America* 115, E11827–E11836 (2018).

606 15. O'Brown, N. M., Megason, S. G. & Gu, C. Suppression of transcytosis regulates zebrafish
607 blood-brain barrier function. *eLife* 8, 41 (2019).

608 16. Xie, J., Farage, E., Sugimoto, M. & Anand-Apte, B. A novel transgenic zebrafish model for
609 blood-brain and blood-retinal barrier development. *BMC developmental biology* 10, 76 (2010).

610 17. Miller, A. C., Obholzer, N. D., Shah, A. N., Megason, S. G. & Moens, C. B. RNA-seq-based
611 mapping and candidate identification of mutations from forward genetic screens. *Genome*
612 *research* 23, 679–686 (2013).

613 18. Bonnet, F. *et al.* Structure and cellular distribution of mouse brain testican. Association with
614 the postsynaptic area of hippocampus pyramidal cells. *The Journal of biological chemistry* 271,
615 4373–4380 (1996).

616 19. Edgell, C.-J. S., BaSalamah, M. A. & Marr, H. S. Testican-1: a differentially expressed
617 proteoglycan with protease inhibiting activities. *International review of cytology* 236, 101–122
618 (2004).

619 20. Ben-Zvi, A. *et al.* Mfsd2a is critical for the formation and function of the blood-brain barrier.
620 *Nature* 509, 507–511 (2014).

621 21. Guo, L., Zhang, H., Hou, Y., Wei, T. & Liu, J. Plasmalemma vesicle-associated protein: A
622 crucial component of vascular homeostasis. *Exp Ther Med* 12, 1639–1644 (2016).

623 22. Charbonnier, F. *et al.* Expression of the proteoglycan SPOCK during mouse embryo
624 development. *Mechanisms of development* 90, 317–321 (2000).

625 23. Raj, B. *et al.* Emergence of Neuronal Diversity during Vertebrate Brain Development.
626 *Neuron* 1–24 (2020) doi:10.1016/j.neuron.2020.09.023.

627 24. Armulik, A., Genové, G. & Betsholtz, C. Pericytes: Developmental, Physiological, and
628 Pathological Perspectives, Problems, and Promises. *Developmental cell* 21, 193–215 (2011).

629 25. Bell, R. D. *et al.* Pericytes control key neurovascular functions and neuronal phenotype in
630 the adult brain and during brain aging. *Neuron* 68, 409–427 (2010).

631 26. Wang, Y., Pan, L., Moens, C. B. & Appel, B. Notch3 establishes brain vascular integrity by
632 regulating pericyte number. *Development (Cambridge, England)* 141, 307–317 (2013).

633 27. Daneman, R., Zhou, L., Kebede, A. A. & Barres, B. A. Pericytes are required for blood-brain
634 barrier integrity during embryogenesis. *Nature* 468, 562–566 (2010).

635 28. Chen, J. *et al.* CD146 coordinates brain endothelial cell–pericyte communication for blood–
636 brain barrier development. *Proc National Acad Sci* 114, E7622–E7631 (2017).

637 29. Westerfield, M. The zebrafish book: a guide for the laboratory use of zebrafish (Brachydanio
638 rerio). (1993).

639 30. Chi, N. C. *et al.* Foxn4 directly regulates tbx2b expression and atrioventricular canal
640 formation. *Genes & Development* 22, 734–739 (2008).

641 31. Ando, K. *et al.* Clarification of mural cell coverage of vascular endothelial cells by live
642 imaging of zebrafish. *Development (Cambridge, England)* 143, 1328–1339 (2016).

643 32. Li, B. & Dewey, C. N. RSEM: accurate transcript quantification from RNA-Seq data with or
644 without a reference genome. *BMC bioinformatics* 12, 323 (2011).

645 33. Choi, H. M. T. *et al.* Third-generation in situ hybridization chain reaction: multiplexed,
646 quantitative, sensitive, versatile, robust. *Development (Cambridge, England)* 145, (2018).

647 34. Pomreinke, A. P. *et al.* Dynamics of BMP signaling and distribution during zebrafish dorsal-
648 ventral patterning. *Elife* 6, e25861 (2017).

649 35. Bresciani, E., Broadbridge, E. & Liu, P. P. An efficient dissociation protocol for generation of
650 single cell suspension from zebrafish embryos and larvae. *Methodsx* 5, 1287–1290 (2018).

651 36. McGinnis, C. S. *et al.* MULTI-seq: sample multiplexing for single-cell RNA sequencing using
652 lipid-tagged indices. *Nat Methods* 16, 619–626 (2019).

653 37. Klein, A. M. *et al.* Droplet Barcoding for Single-Cell Transcriptomics Applied to Embryonic
654 Stem Cells. *Cell* 161, 1187–1201 (2015).

655 38. Wagner, D. E. *et al.* Single-cell mapping of gene expression landscapes and lineage in the
656 zebrafish embryo. *Science* 108, eaar4362-13 (2018).

657 39. Traag, V. A., Waltman, L. & Eck, N. J. van. From Louvain to Leiden: guaranteeing well-
658 connected communities. *Sci Rep-uk* 9, 5233 (2019).

659 40. Weinreb, C., Wolock, S. & Klein, A. M. SPRING: a kinetic interface for visualizing high
660 dimensional single-cell expression data. *Bioinformatics* 34, 1246–1248 (2017).

661